Biochimica et Biophysica Acta 1817 (2012) 1063–1071

Contents lists available at SciVerse ScienceDirect

Biochimica et Biophysica Acta

journal homepage: www.elsevier.com/locate/bbabio

Structural backgrounds for the formation of a catalytically competent complex with NADP(H) during hydride transfer in ferredoxin–NADP$^+$ reductases

Ana Sánchez-Azqueta [a], Matías A. Musumeci [b], Marta Martínez-Júlvez [a], Eduardo A. Ceccarelli [b,*], Milagros Medina [a,**]

[a] Departamento de Bioquímica y Biología Molecular y Celular, Facultad de Ciencias, and Institute of Biocomputation and Physics of Complex Systems, Universidad de Zaragoza, Spain
[b] Molecular Biology Division, Instituto de Biología Molecular y Celular de Rosario (IBR), Facultad de Ciencias Bioquímicas y Farmacéuticas, Universidad Nacional de Rosario, Argentina

ARTICLE INFO

Article history:
Received 1 March 2012
Received in revised form 11 April 2012
Accepted 12 April 2012
Available online 20 April 2012

Keywords:
Ferredoxin–NADP$^+$ reductase
Stopped-flow
X-ray structure
Protein–ligand interaction
Catalytically competent complex
Hydride transfer

ABSTRACT

The role of the highly conserved C266 and L268 of pea ferredoxin–NADP$^+$ reductase (FNR) in formation of the catalytically competent complex of the enzyme with NADP(H) was investigated. Previous studies suggest that the volume of these side-chains, situated facing the side of the C-terminal Y308 catalytic residue not stacking the flavin isoalloxazine ring, may be directly involved in the fine-tuning of the catalytic efficiency of the enzyme. Wild-type pea FNR as well as single and double mutants of C266 and L268 residues were analysed by fast transient-kinetic techniques and their midpoint reduction potentials were determined. For the C266A, C266M and C266A/L268A mutants a significant reduction in the overall hydride transfer (HT) rates was observed along with the absence of charge-transfer complex formation. The HT rate constants for NADPH oxidation were lower than those for NADP$^+$ reduction, reaching a 30-fold decrease in the double mutant. In agreement, these variants exhibited more negative midpoint potentials with respect to the wild-type enzyme. The three-dimensional structures of C266M and L268V variants were solved. The C266M mutant shows a displacement of E306 away from the relevant residue S90 to accommodate the bulky methionine introduced. The overall findings indicate that in FNR the volume of the residue at position 266 is essential to attain the catalytic architecture between the nicotinamide and isoalloxazine rings at the active site and, therefore, for an efficient HT process. In addition, flexibility of the 268–270 loop appears to be critical for FNR to achieve catalytically competent complexes with NADP(H).

1. Introduction

Ferredoxin (flavodoxin)-NADP(H) reductases (FNR) are ubiquitous flavoenzymes that deliver NADPH or low-potential one-electron donors to redox-based metabolic reactions in plastids, mitochondria and bacteria. Plastidic FNRs efficiently catalyse the electron transfer from ferredoxin (Fd) to NADP$^+$ via its flavin cofactor, while related enzymes from organisms with heterotrophic metabolism or anoxygenic photosynthesis display lower turnover numbers than those of their plastidic and cyanobacterial homologues [1–3]. Structural features of these enzymes, yet to be explained, must contribute to such differential behaviours. In plastidic FNRs the final hydride transfer (HT) event between its flavin cofactor and the pyridine nucleotide is a reversible process that involves the formation of two transient charge-transfer complexes: FNR_{ox}–NADPH (CTC-1) and FNR_{hq}–NADP$^+$ (CTC-2), characterised by the appearance of broad spectral bands centred at ~600 nm and ~800 nm, respectively. These complexes are formed prior and upon HT whatever the HT direction [4–7], suggesting that during HT an approach of the N5 donor/acceptor atom of the FADH$^-$ isoalloxazine (N5i) from FNR to the C4 acceptor/donor of the coenzyme nicotinamide ring (C4n) occurs through some stacking [6,8]. Mutations either preventing or improving the stacking between the isoalloxazine and the nicotinamide rings with regard to the WT system have been related to low efficiency in the HT reaction [5,6,9–11]. The highly conserved Tyr at the C-terminal position in plastidic FNRs has been reported as a key element to modulate the strong stacking tendency between the isoalloxazine and nicotinamide rings in the catalytically competent complex [2,5]. Molecular dynamic simulations have provided theoretical structures

Abbreviations: FNR, ferredoxin–NADP$^+$ reductase; FNR_{ox}, FNR in the oxidised state; FNR_{hq}, FNR in the hydroquinone reduced state; WT, wild-type; r.m.s.d., root mean square deviation; NMN, nicotinamide mononucleotide portion of NAD(P)$^+$/H; 2′P-AMP, 2′-phospho-AMP portion of NADP$^+$/H; HT, hydride transfer; CTC, charge-transfer complex; $k_{A\rightarrow B}$, $k_{B\rightarrow C}$, apparent conversion rate constants derived by global analysis; k_{HT}, k_{HT-1}, first-order hydride transfer rate constants for the forward and backward reactions, respectively; TRIS, tris(hydroxymethyl)aminomethane; EDTA, ethylenediaminetetraacetic acid; PEG, polyethylene glycol; HEPES, 4-(2-hydroxyethyl)-1-piperazineethanesulfonic acid

* Correspondence to: E.A. Ceccarelli, IBR, CONICET, Facultad de Ciencias Bioquímicas y Farmacéuticas, UNR, Suipacha 531. S2002LRK Rosario, Argentina. Tel.: +54 341 4351235; fax: +54 341 4390465.
** Correspondence to: M. Medina, Departamento de Bioquímica y Biología Molecular y Celular, Facultad de Ciencias, Pedro Cerbuna 12, Universidad de Zaragoza, 50009-Zaragoza, Spain. Tel.: +34 976 762476; fax: +34 976 762123.
E-mail addresses: ceccarelli@ibr.gov.ar (E.A. Ceccarelli), mmedina@unizar.es (M. Medina).

0005-2728/$ – see front matter © 2012 Elsevier B.V. All rights reserved.
doi:10.1016/j.bbabio.2012.04.009

for the putative WT FNR_{hq}–$NADP^+$ and FNR_{ox}–NADPH catalytically competent complexes. These models allocate the C-terminal Tyr side-chain breaking the parallelism and decreasing the stacking between the isoalloxazine and the nicotinamide rings, while keeping the reacting atoms N5i and C4n at a HT distance [12]. Such control of the stacking increases the N5i-hydride–C4n angle, producing the near co-linear disposition as expected for an efficient HT process. In plastidic FNRs the C-terminal Tyr is constrained against the isoalloxazine by a Cys and a Leu highly conserved at the $NADP^+$ binding motif (C266 and L268 in pea FNR and C261 and L263 in *Anabaena* FNR). The volume of these amino acids has been shown to contribute to the fine-tuning of the catalytic efficiency of the enzyme [13,14]. The thiol of the Cys residue is usually pointing towards the active site, in the environment of the Ser, Glu and C-terminal Tyr residues conserved in all known FNRs and other members of this family [1,12,15,16]. Molecular dynamic simulations of the putative catalytically competent structures of the *Anabaena* enzyme suggest that the N7 atom of the nicotinamide amide (N7n) might interact with E301 and S80 (E306 and S90 in pea FNR), whereas C261 and S80 side chains might stabilise the position of the C4n, the atom from the coenzyme involved in the HT reaction. Simultaneously, L263 gets displaced with regard to the free structure to interact with the ribose of the nicotinamide mononucleotide portion of the coenzyme (NMN), and to narrow the cavity in which the 2′-P-AMP moiety of the coenzyme gets sandwiched between L263 and the aromatic ring of Y235 (Y240 in pea FNR). In this work structural and biochemical studies were combined to understand the implication of these Leu and Cys residues in both the modulation of the midpoint reduction potential of the flavin cofactor and in the formation of the architecture of the catalytically competent complexes.

2. Materials and methods

2.1. Production of enzyme samples

The WT pea FNR and its L268V, C266M, C266L, C266A, C266A/L268A mutants were produced as previously reported [14]. Photoreduction of the FNR variants was performed at 25 °C in 50 mM tris(hydroxymethyl) aminomethane/HCl (TRIS/HCl) pH 8.0 under anaerobic conditions. Typically, the cell contained ~20 μM FNR, 3 mM ethylenediaminetetraacetic acid (EDTA) and 1–5 μM 5-deazariboflavin. Stepwise reduction was achieved by light irradiation from a 250 W slide projector for different periods of time. After each irradiation the UV–vis spectrum was recorded in a Cary 100 spectrophotometer. The maximum percentage of semiquinone stabilised was inferred from the plot of the absorbance maximum at band-I for the oxidised flavoprotein *versus* the absorbance at the maximum of the neutral semiquinone [17,18]. FNR_{hq} was similarly produced for transient-state measurements and midpoint-reduction potential determinations [7].

2.2. Determination of midpoint reduction potentials of the FNR variants

Midpoint reduction potentials for the ox/hq couple ($E_{ox/hq}$) of WT, C266A and C266A/L268A FNR variants were determined at 25 °C by potentiometric titration under anaerobic conditions using a calomel electrode as reference ($E_m = -244.4$ mV at 25 °C). Typically, the solution contained ~20 μM FNR, 50 mM TRIS/HCl buffer, pH 8.0, 5% glycerol, 0.02% n-dodecyl-β-D-maltoside, 3 mM EDTA and 2 μM 5-deazariboflavin. Methylviologen ($E_m = -446$ mV), benzylviologen ($E_m = -359$ mV) and anthraquinone-2-sulfonate ($E_m = -225$ mV) were additionally introduced as mediators at 1 μM. Stepwise reduction of the protein was achieved by photoreduction using the equipment previously described [19]. The system was considered equilibrated when the potential (E), measured with a Fluke 177 true-RMS multimeter, remained stable for at least 10 min. The UV–vis absorbance spectrum was then recorded and used to determine [FNR_{ox}] and [FNR_{hq}] at the equilibrium after each reduction step. $E_{ox/hq}$ was calculated by linear regression analysis according to the Nernst Equation:

$$E = E_{ox/hq} + (0.056/n)\log\left([FNR_{ox}]/[FNR_{hq}]\right) \quad (1)$$

where n is the number of electrons transferred. The theoretical values of each one-electron single step, $E_{ox/sq}$ and $E_{sq/hq}$, were derived from Eqs. (2) and (3)

$$E_{ox/sq} - E_{sq/hq} = 0.11\log(2[SQ]/(1-[SQ])) \quad (2)$$

$$\left(E_{ox/sq} + E_{sq/hq}\right)/2 = E_{ox/hq} \quad (3)$$

using the experimentally determined $E_{ox/hq}$ and the molar fraction of the maximum percentage of SQ stabilised. Errors in the $E_{ox/hq}$, $E_{ox/sq}$ and $E_{sq/hq}$ determined were estimated to be ±5 mV.

2.3. Stopped-flow pre-steady-state kinetic measurements

Reactions between $NADP^+$/H and the $FNR_{hq/ox}$ variants were analysed by following the absorption spectral evolution in the 400–1000 mm region using an Applied Photophysics SX17.MV stopped-flow equipped with a photodiode array detector as previously described [5]. Reactions were performed in 50 mM TRIS/HCl, pH 8.0, at 6 °C and under anaerobic conditions, with final FNR concentrations of ~20 μM, while the nucleotide concentration was in the 20–200 μM range. Under these conditions, the instrument dead time was 2–3 ms. Multiple wavelength absorption data were collected and processed using the X-Scan software (Appl. Phot. Ltd.). Typically, 400 spectra per second were collected. Global analysis and numerical integration methods using Pro-Kineticist (Appl. Phot. Ltd.) were applied to the collected data corresponding to the spectral information obtained along the reaction time, fitting them to either a single step, A → B, or a two step, A → B → C, model. This allowed estimation of the conversion rate constants ($k_{A\to B}$, $k_{B\to C}$), as well as obtaining spectral information of intermediate species [7]. The single step mechanism sometimes applied when a previous reaction occurred within the instrumental dead-time, and can, therefore, not been observed in our experiment despite its existence. In these cases a B → C model was assumed to indicate that a previous reaction (A → B) was required to occur to allow the observed reaction to take place. A, B and C are spectral species, reflecting a distribution of enzyme intermediates (reactants, CTCs, products, Michaelis complexes) at any certain time along the course of the enzyme:coenzyme interaction and HT processes, and do not necessarily represent a single distinct enzyme intermediate. Moreover, none of them represents individual species and, their spectra cannot be included as fixed in the global-fitting. Model validity was assessed by lack of systematic deviations from residual plots at different wavelengths, inspection of calculated spectra and consistency among the number of significant singular values with the fit model. In some cases, $k_{A\to B}$ rate constants derived from experimental data show dependence profiles on the $NADP^+$/H concentration that fit properly to the equation describing binding at a single site followed by the HT processes,

$$k_{A\to B} = \frac{k_{HT-1}(K_d + [NADP^+/H]) + k_{HT}[NADP^+/H]}{[NADP^+/H] + K_d} \quad (4)$$

and allow the determination of the dissociation (K_d) and the HT rate constants for the forward and backward reactions (k_{HT}, $k_{HT\text{-}1}$). However, the experimental rate constants were independent on the enzyme concentration for most of the analysed processes and could be related with k_{HT} or $k_{HT\text{-}1}$ minimal values. Errors in the estimated values of K_d and k_{HT} values were ±20% and ±15%, respectively.

2.4. Crystal growth, data collection and structure refinement

Despite that different crystallisation conditions were screened using several *Jena Bioscience* grids for all studied pea FNR mutants, only crystals of C266M and L268V FNRs were suitable to obtain X ray diffraction data sets. Crystals of C266M FNR were generated in droplets of 0.5 μL containing 0.25 μL of 4.1 mg/mL of protein in 5 mM potassium phosphate, pH 8.0, and 0.25 μL of the reservoir solution containing 15% polyethylene glycol (PEG) 1.5 K. Crystals for the L268V variant grew from drops of 1 μL of a 5.8 mg/mL protein solution in 5 mM potassium phosphate, pH 8.0, and 2 μL of 10% PEG 6 K, 5% 2-methyl-2,4-pentanediol and 0.1 M (4-(2-hydroxyethyl)-1-piperazineethanesulfonic acid (HEPES), pH 7.5. Drops were equilibrated against 60 μL and 500 μL of reservoir solutions, respectively, at 18 °C. Cryoprotectants consisted of the mother liquid supplemented with 25–30% glycerol. Diffraction data sets were collected at 100 K on the ID14.4 and BM16 lines at ESRF (Grenoble, France), and were processed with XDS [20] and scaled and reduced with SCALA from CCP4i [21,22]. Both structures were solved by MOLREP [23] from CCP4i using WT pea FNR (1QG0) as model [10]. The generated single solutions were refined with REFMAC 5.5 [24], using TLS refinement in the last steps [25]. This process was alternated with manual model building with Coot [26]. PROCHECK [27] and MOLPROBITY [28] were used to assess final structures. Both FNR crystals belonged to the $P2_12_12_1$ orthorhombic space group, and their V_m were 3.31 and 3.41 $Å^3$/Da, respectively, with two FNR molecules in the asymmetric unit and 62.9 and 63% solvent content. Unit cell dimensions and other experimental data are detailed in Table 1. Each molecule of models comprised residues 13–308, 1 FAD and some water molecules. More than 99% of the residues in the Ramachandran plots fall within the allowed regions. Coordinates and structure factors are deposited in PDB with PDB ID: 4AF6 for L268V and PDB ID: 4AF7 for C266M.

Table 1
Data collection and refinement statistics for C266M and L268V FNRs. Values in parentheses refer to the highest resolution shell.

Crystal data	C266M	L268V
Space group	$P2_12_12_1$	$P2_12_12_1$
Unit cell parameters (Å)	73.74	73.98
	91.73	94.70
	139.58	138.93
Data collection		
Temperature (K)	100	100
Beam line	ID14.4 ESRF	BM16 ESRF
Wavelength (Å)	0.99993	0.93362
Resolution (Å)	46.53–2.85 (3.00–2.85)	24.67–2.90 (3.06–2.90)
Total reflections	118,836	159,610
Unique reflections	22,623 (3223)	22,283 (3199)
Mean $I/\sigma(I)$	11.9 (3.2)	11.0 (2.2)
Completeness (%)	99.3 (99.5)	99.8 (100)
Redundancy	5.3 (5.4)	7.2 (7.3)
R_{merge} [a]	0.094 (0.449)	0.116 (0.604)
Data refinement		
Resolution range (Å)	50–2.85	50–2.9
Protein non-hydrogen atoms	4708	4712
Ligand non-hydrogen atoms	106	106
Solvent non-hydrogen atoms	19	28
R_{work} (%)	23.9	24.1
R_{free} [b](%)	29.8	28.4
r.m.s.d. bond length, Å	0.008	0.008
r.m.s.d. bond angles, °	1.120	1.064
Average B-factor, $Å^2$	42.8	39.3

[a] $R_{sym} = \Sigma|I - I_{av}|/\Sigma I$, where the summation is over symmetry-equivalent reflection.
[b] R calculated for 7% of data excluded from the refinement.

3. Results

3.1. Photoreduction properties and midpoint reduction potentials of the pea FNR variants

The spectral shape, the maxima positions and the amount of maximal semiquinone stabilised (12–20%) along with the photoreduction of the L268V, C266A and C266A/L268A pea FNR variants were similar to those for WT (Fig. 1A). However, the same treatment induced FAD dissociation and protein denaturation for the C266M and C266L variants. $E_{ox/hq}$ values were determined by potentiometric titration for the stable FNR forms upon photoreduction (Fig. 1B, Table 2). $E_{ox/sq}$ and $E_{sq/hq}$ were derived from Eqs. (2) and (3) taking into account the maximal amount of semiquinone stabilised by each variant. The $E_{ox/hq}$ for WT pea FNR was −342 mV. This value is slightly less negative than those reported for *Anabaena* and spinach FNRs under similar conditions. Accordingly, in the enzymes from those species the predicted $E_{sq/hq}$ is more negative than in pea FNR. Therefore, in the latter enzyme the FAD semiquinone appears to be thermodynamically destabilised as in other FNRs. No changes in these parameters were obtained for the L268V variant, but replacement of C266 with Ala shifted $E_{ox/hq}$, $E_{ox/sq}$ and $E_{sq/hq}$ to more negative values (Table 2).

3.2. Formation and stabilisation of intermediate species upon HT reactions with the coenzyme on WT and mutant FNR forms

Transient kinetics for the reactions of WT and L268V FNR_{ox} with NADPH were consistent with formation within the experimental dead-time of two bands centred at ~620 nm and ~900 nm (Fig. 2A, B), in agreement with the formation of CTC-1 and CTC-2, respectively, as reported in other FNR species [5,6]. Simultaneously, the decrease in the flavin band-I indicates HT and reduction of some FNR molecules. Subsequent spectral evolution indicates additional HT, with conversion of CTC-1 into CTC-2 until an equilibrium was reached in a process that fits a B→C model (inset Fig. 2A, B). On the contrary, reduction of C266M, C266L, C266A and C266A/L268A FNRs by NADPH occurred

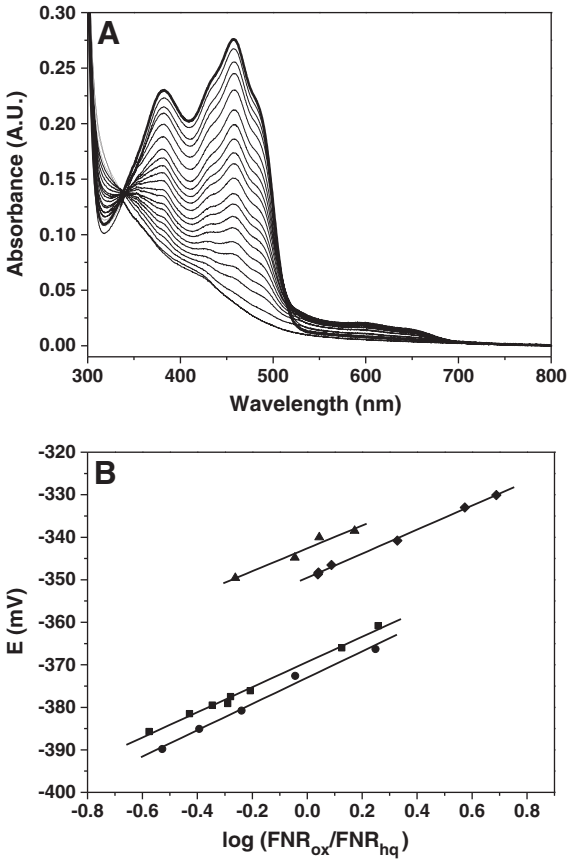

Fig. 1. A. Absorbance spectra obtained during the photoreduction of C266A FNR. B. Nernst plots for the redox titrations of WT (▲), L268V (♦), C266A (●) and C266A/L268A (■) pea FNRs. Experimental conditions described in Materials and methods.

Table 2
Midpoint reduction potentials for the different FNR variants. Measurements in 50 mM TRIS/HCl, pH 8.0, with 5% glycerol, 0.02% n-dodecyl-β-D-maltoside at 25 °C. Errors in the $E_{ox/hq}$, $E_{ox/sq}$ and $E_{sq/hq}$ determined were estimated to be ±5 mV.

	$E_{ox/hq}$ (mV)	$E_{ox/sq}$[a](mV)	$E_{sq/hq}$[a](mV)	% SQ
pea FNR	−342	−373	−311	12
L268V	−349	−370	−328	17
C266A	−373	−396	−350	16
C266A/L268A	−370	−387	−353	20
Anabaena FNR[b]	−374	−385	−371	27
spinach FNR[c]	−380	−402	−358	16
FAD[d]	−241	−373	−109	0.2

[a] Calculated from Eqs. (2) and (3) as indicated in the text.
[b] Data from [41], obtained by photoreduction in 50 mM TRIS/HCl, pH 8.0, at 25 °C.
[c] Data from [42], obtained in 50 mM HEPES, pH 8.0, with 15% glycerol at 10 °C.
[d] Data from [43].

with an undetectable appearance in the 600–1000 nm spectral region of nicotinamide–isoalloxazine CTC intermediates. Moreover, since mutations on C266 cause drastic changes in the interaction of the pea FNR with $NADP^+$/H, the spectroscopic properties of intermediate CTC of the mutants might differ from those of WT, being even undetectable, and, therefore, the assignment of transient spectra should be taken with care. Processes with C266L and C266M fit to an A → B model, with species that display spectroscopic properties of FNR_{ox} and FNR_{hq}, respectively (Fig. 2C). The broad absorption band over 550 nm appearing in the C266L spectrum after anaerobic treatment relates to a small percentage of protein denaturation due to its lower stability under these conditions. At difference, the process for C266A was best fitted to a two step model, A → B → C (Fig. 2D). Conversion of A into B is consistent with a small degree of protein reduction. Unexpectedly, upon transformation of B into C semiquinone formation is observed. Noticeably, formation of semiquinone is also observed from the first detectable measurement for the process with C266A/L268A FNR_{ox} (not shown), also consistent with a two step model. It is unusual that NADPH, which is an obligate two-electron donor, is capable of producing flavin semiquinone under anaerobic conditions. However, reductive titrations with pyridine nucleotides showing the formation of enzyme species with spectral characteristics typical of a neutral FAD semiquinone have been reported for some members of the FNR family, as WT FprA from *Mycobacterium tuberculosis* or mammalian adrenodoxin reductase. In those cases the semiquinone stabilisation was previously assigned to binding of the coenzyme to both the oxidised and hydroquinone forms of the enzyme followed by fast electronic disproportionation between pairs of such molecules [29,30]. Therefore, processes for C266A and C266A/L268A ended with the accumulation of neutral semiquinone and almost no flavin reduction, while a considerable degree of flavin reduction was observed for the C266L and C266M variants.

Reduction of $NADP^+$ by WT and L268V FNR_{hq} variants occurred with the appearance of a considerable amount of the typical CTC-2 spectrum and the appearance of traces of CTC-1 species within the instrumental dead time. Subsequently, band-I of the flavin increased consistently with protein oxidation and transformation of CTC-2 into CTC-1, fitting the overall process to a two step model (Fig. 3A and B). All the C266A and C266A/L268A FNR_{hq} samples showed spectroscopic properties indicating a small proportion of the neutral semiquinone when placed in the stopped-flow instrument and previous to the mixing with the coenzyme. We relate this behaviour to the more negative midpoint reduction potential for these variants as

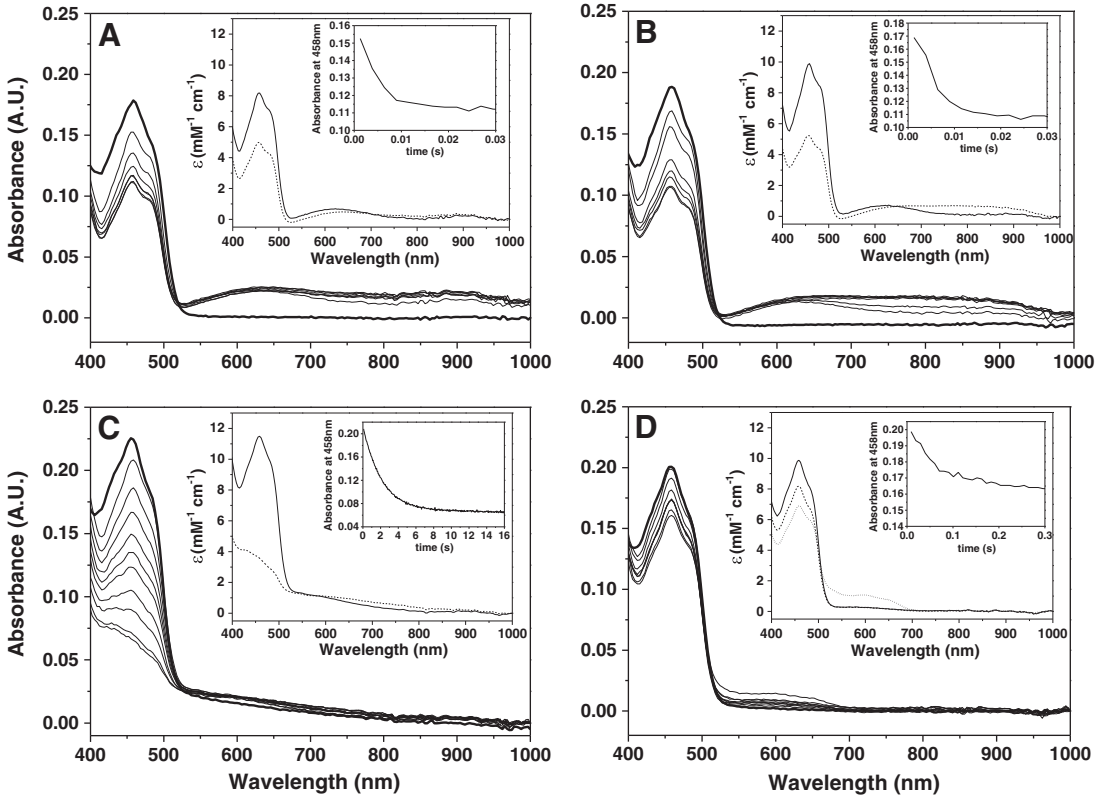

Fig. 2. Spectral evolution during the reduction by NADPH of the different FNR_{ox} variants. (A) WT FNR_{ox}; spectra recorded at 0.00128, 0.00384, 0.0064, 0.00896, 0.01152 and 0.024 s after mixing. (B) L268V FNR_{ox}; spectra recorded at 0.00128, 0.00384, 0.0064, 0.00896, 0.01152 and 0.024 s. (C) C266L FNR_{ox}; spectra recorded at 0.08064, 0.4493, 0.8589, 1.268, 1.678, 2.088, 2.907, 4.136, 8.232 and 16.38 s. (D) C266A FNR_{ox}; spectra recorded at 0.00896, 0.2944, 0.4992, 0.0704, 0.09088, 0.1114, 0.2138 and 0.4186 s. In all cases, final concentrations for FNR_{ox} and NADPH are 20 μM and 100 μM, respectively. The thick line is the spectrum of the oxidised protein before mixing. The inset shows the absorbance spectra for the two (in A, B and C) or three (in D) transient-state kinetically distinguishable species obtained by global analysis. The second inset shows the time evolution of the absorption at 458 nm.

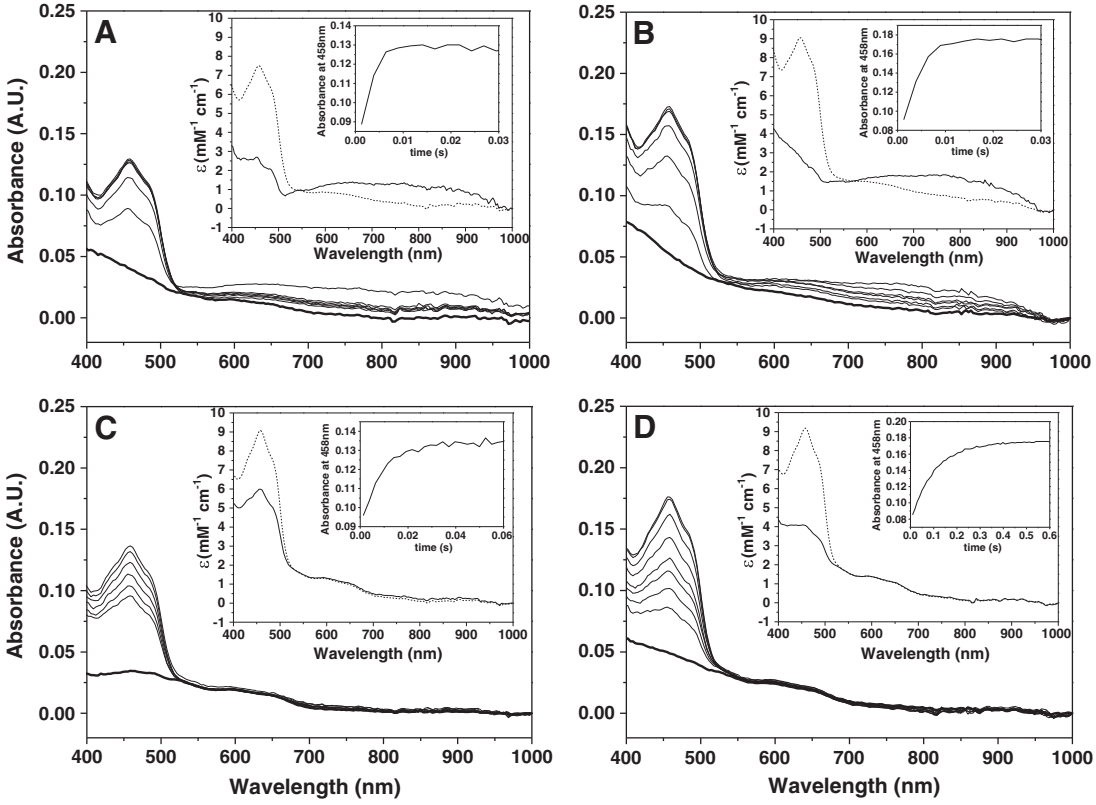

Fig. 3. Spectral evolution during the reduction of $NADP^+$ by the different FNR_{hq} variants. (A) WT FNR_{hq}; spectra recorded at 0.00128, 0.00384, 0.0064, 0.00896, 0.01152 and 0.024 s. (B) L268V FNR_{hq}; spectra recorded at 0.00128, 0.00384, 0.0064, 0.00896, 0.01152 and 0.024 s. (C) C266A FNR_{hq}; spectra recorded at 0.00128, 0.00384, 0.0064, 0.01152, 0.02688 and 0.05248 s. (D) C266A/L268A FNR_{hq}; spectra recorded at 0.00896, 0.02944, 0.04992, 0.0704, 0.1114, 0.2138 and 1.033 s. In all cases, final concentrations for FNR_{hq} and $NADP^+$ are 20 μM and 100 μM, respectively. The thick line is the spectrum of the fully reduced protein before the mixing. The inset shows the absorbance spectra for the two pre-steady-state kinetically distinguishable species obtained by global analysis. The second inset shows the time evolution of the absorption at 458 nm.

compared with the WT enzyme and to their fully reduced state being less stable which may induce disproportionation as mentioned above. Therefore, measurements of the processes with $NADP^+$ were started assuming the presence of some semiquinone. These processes evolved without the spectral detection of any CTC intermediate. At the equilibrium the initial amount of semiquinone together with the protein oxidised form was observed (Fig. 3C and D). Finally, the low stability of photoreduced C266L and C266M FNRs prevented the analysis of the HT process to the coenzyme in these variants.

3.3. Hydride transfer efficiency for the FNR variants

Global analysis of data obtained at different coenzyme concentrations indicated that, with the only exception of the reduction of C266A by NADPH, all examined processes best fitted a one-step mechanism. Reactions for the WT and L268V variants corresponded to the evolution of a species previously produced in the instrumental death time, corresponding, therefore, to a $B \rightarrow C$ model, as already reported for *Anabaena* WT FNR [5,6,13]. $k_{B\rightarrow C}$ values at a particular coenzyme concentration are shown in Table 3. $k_{B\rightarrow C}$ values were independent of the coenzyme concentration for the reactions of WT and L268V FNR_{ox} with NADPH, as well as for the reaction of L268V FNR_{hq} with $NADP^+$. Therefore, and as previously reported [5], these $k_{B\rightarrow C}$ values can be related with the HT rate constant minimal values, k_{HT} or $k_{HT\text{-}1}$, for the photosynthetic and reverse reactions, respectively (Table 4). The hyperbolic behaviour shown by the observed rate constants as a function of the coenzyme concentration for the processes of WT and C266A FNR_{hq} with $NADP^+$ allowed data fitting by using the analytical solution of the differential equations describing a two step mechanism [7] and therefore, to determine dissociation or

Table 3
Observed transient-rate constants for the reaction of pea $FNR_{hq/ox}$ variants with $NADP^+$/H. Data from kinetics obtained at $FNR_{hq/ox}$:$NADP^+$/H ratio of 1:5 and 6 °C. Errors in the estimated $k_{A\rightarrow B}$ and $k_{B\rightarrow C}$ were ±15%.

	FNR_{ox} and NADPH		FNR_{hq} and $NADP^+$	
	$k_{A\rightarrow B}$ (s^{-1})	$k_{B\rightarrow C}$ (s^{-1})	$k_{A\rightarrow B}$ (s^{-1})	$k_{B\rightarrow C}$ (s^{-1})
WT		275		400
L268V		270		260
C266L	0.45		n.d.[a]	
C266M	0.13		n.d.[a]	
C266A	18	1.5	120	
C266A/L268A		0.72	10.2	

[a] n.d., Not determined due to the lack of stability of FNR_{hq} for these variants.

Table 4
Transient-state kinetic parameters for the hydride transfer between $FNR_{hq/ox}$ and $NADP^+$/H. Kinetic parameters derived from observed transient-rate constants as a function of the coenzyme concentration in TRIS/HCl 50 mM pH 8.0 and 6 °C. Errors in the estimated K_d and k_{HT} were ±15%.

FNR form	FNR_{ox} and NADPH		FNR_{hq} and $NADP^+$	
	K_d^{NADPH} (μM^{-1})	k_{HT} (s^{-1})	K_d^{NADP+} (μM^{-1})	$k_{HT\text{-}1}$ (s^{-1})
Pea WT		291.3	16.6	462.7
L268V		274.5		254.1
C266L		0.49		n.d.
C266M		0.14		n.d.
C266A	>39.7[b]	27.1[b]	34.9	147.3
C266A/L268A		0.86	>224.1[b]	27.2[b]
Anabaena WT[a]		300		285

[a] Data from [6].
[b] Saturation was not fully reached and approximate parameters can only be reported.

rearrangement constants, K_d^{NADP+}, as well as the HT rate constants (Fig. 4A, Table 4). For the processes of C266A FNR_{ox} with NADPH and C266A/L268A FNR_{hq} with $NADP^+$ (Fig. 4B) the hyperbolic dependence is just envisaged, saturation is not reached and only apparent K_d^{NADP+}, K_d^{NADPH}, k_{HT} and k_{HT-1} minimal parameters can be reported (Table 4). The obtained values indicate a very fast HT from WT FNR to the coenzyme. However, the K_d^{NADP+} value obtained for WT pea FNR appears lower than those obtained with FNRs from other sources [5] and even with the pea L268V variant. Nevertheless, despite the stronger binding, replacement of L268 with Val decreases k_{HT-1} by 1.5-fold (Table 4). Rates for the reduction of C266L and C266M FNR_{ox} by NADPH corresponded to the direct conversion of reactants into products, $k_{A\rightarrow B}\sim k_{HT}$, without the appearance of intermediate CTC species, in very inefficient processes. Reduction of C266A by NADPH was described by two rate constants, while the reverse process corresponded to a single one, probably including the whole reaction. These parameters for the C266 mutants, together with the lack of detection of the typical CTC and the reported increased K_m^{NADPH} values [14], indicate that replacement of C266 by Ala impedes the catalytically competent binding of the coenzyme. Additionally, the HT rates for the forward and backward reactions are differentially affected, resulting in a drastic decrease of the reaction in the non-photosynthetic direction. Taken together these results suggest that the mutation of C266 in FNR has a deleterious influence in the rate of the binding of $NADP^+$/H to FNR and/or in the production of the catalytic competent architecture between the isoalloxazine and nicotinamide rings for efficient HT. The additional replacement of L268 by Ala in the C266A mutant also contributes to both effects. A minor decrease of $k_{B\rightarrow C}$ with the coenzyme concentration was observed for the reactions of WT FNR_{ox} with NADPH, and of L268V, C266M and C266A FNR_{hq} with $NADP^+$ (not shown), as already described for FNRs from other sources as well as in other related oxidoreductases [7,31]. This effect could be related to enzyme inhibition consistent with a simple single-binding-site model in which reversible HT causes the observed effect.

3.4. Crystal structure of the C266M and L268V FNR variants

The C266M and L268V FNRs structures were refined up to 2.85 and 2.9 Å resolutions respectively, with final R and R_{free} factors of 23.9 and 29.8, and 24.1 and 28.4 (Table 1). Each asymmetric unit contains two monomers with overall structures similar to that of the WT enzyme (0.37 Å r.m.s.d. (C266M) and 0.32 Å r.m.s.d. (L268V), superimposing the Cα of 296 residues), and models for both mutants included residues 13–308. The most remarkable difference was detected upon replacement of C266 with Met. The position of the S atom of the introduced Met side-chain results stabilised by a dipole–dipole interaction with the main-chain of E306, displacing the terminal β-sheet of FNR outwards the protein core. The new interaction induced a considerable displacement of the E306 side-chain (up to 1.8 Å), increasing the distance between its carboxylate group and the C7 methyl of the isoalloxazine ring by 0.5 Å, and decreasing its accessibility to the active site residues.

4. Discussion

The highly regulated HT process catalysed by FNR from different sources has been thoroughly studied and the role of several amino acid residues systematically investigated. Among them, the volume occupied by the side-chains of L268 and, particularly, C266 is proposed as key to maintain the catalytic efficiency of the pea enzyme [14]. Fast HT reactions between $NADP^+$ and FNR_{hq}, or between NADPH and FNR_{ox}, have been thoroughly studied for the *Anabaena* enzyme [5,7], but so far not reported for pea FNR. Here, we characterise this process using different pea FNR variants at L268 and C266 positions, as well as the WT enzyme itself. Results for the WT pea enzyme are very similar to those of *Anabaena* both in HT rates and stabilisation of CTCs (Fig. 2A and 3A) [5,7].

The C266M and C266L pea FNR variants were unstable upon photoreduction. At variance, reduction by the natural coenzyme, NADPH, unexpectedly stabilised their hydroquinone forms. Therefore, binding of the nucleotide leads to some conformational arrangements in which the enzyme:coenzyme complex is stabilised upon FAD reduction. Moreover, in the equilibrium the amount of reduced form for these species is noticeably higher than for the WT FNR process (Fig. 2C). All mutations in position 266 caused a decrease of HT rates that correlates with changes in the volume of this side-chain (Fig. 5A, C), while spectroscopic formation of CTC species was undetectable. In FNR UV–vis absorbance detection of these CTC intermediates is related with a particular orientation in the overlapping of the nicotinamide and isoalloxazine rings [6]. The architecture of the active centre in FNR has been shown to force a partial stacking of the two reacting rings to allow an effective approach of C4n to N5i, but the closeness of the two rings is not the only requirement for high efficiency in HT. The Y308S (Y303S in *Anabaena*) FNR mutant is unable to catalyse HT as efficiently as the WT enzyme, although the nicotinamide ring binds with strong affinity and it is in a practically planar stack on the isoalloxazine [5,9,10]. Thus, a specific arrangement among the isoalloxazine, the C-terminal Tyr and the nicotinamide of $NADP^+$ is proposed to be necessary to efficiently catalyse HT. This relative orientation appears determined, among other factors, by the steric restrictions established by the C266–L268 FNR residues, facing the side of the C-terminal catalytic Y308 that is not stacking the isoalloxazine ring, and by the tyrosine itself. The lack of CTC detection reported here for the enzymes with mutations on this region is consistent with a decrease of HT rates, and can be related

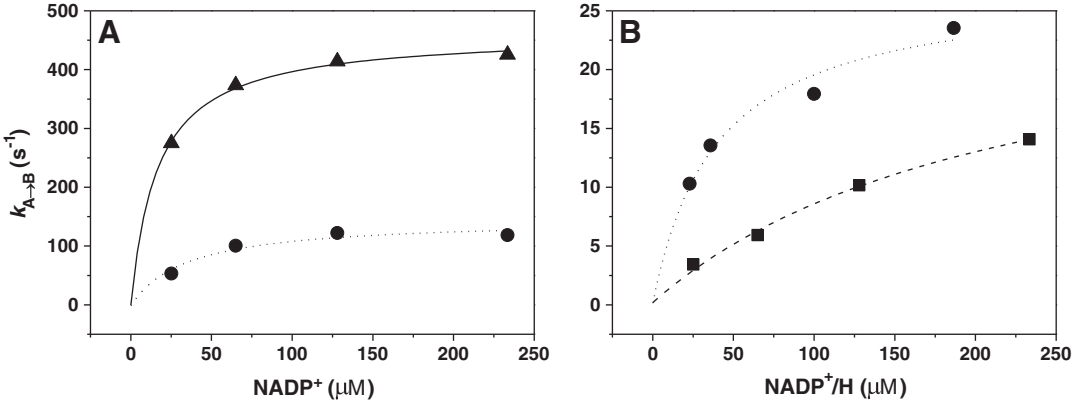

Fig. 4. Experimental conversion rate constants as a function of nucleotide concentration for (A) WT FNR_{hq} (▲, solid line), and C266A FNR_{hq} with $NADP^+$ (●, dotted line) and (B) C266A FNR_{ox} with NADPH (●, dotted line) and C266A/L268A FNR_{hq} with $NADP^+$ (■, dashed line). Fitting of the data was performed using Eq. (4).

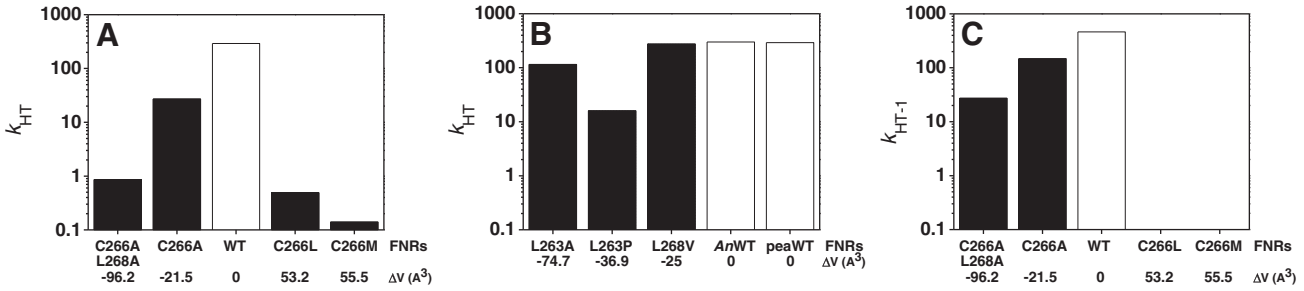

Fig. 5. Hydride transfer first-order rate constants of WT (white bars) and mutant FNRs (black bars) as a function of the volume change in positions (A, C) C266 (include only data from pea FNR) and (B) L268 (include data from pea and *Anabaena* FNRs).

to changes on the nicotinamide environment within the complex [6]. In FNR despite there being no strict correlation between the stability of transient CTCs and the rate of the subsequent HT, either the absence or the very strong stacking between the reacting rings contributes to reduce the efficiency of the HT process [5,6]. Thus, the architecture of the WT FNR active site precisely modulates the stacking probability between the reacting rings in the catalytically competent complex, adjusting the angle and distance between the N5i and the C4n to values that ensure efficient HT processes [12]. Therefore, in our mutants the observed transient-rate constants and the lack of the typical CTCs indicate an overall disruption of the catalytic efficiency. The decrease in HT rates was more pronounced for the reduction of the enzyme by the nucleotide than for the photosynthetic reaction. For WT *Anabaena* [5,7] and pea FNRs the k_{HT-1}/k_{HT} ratio is 1–1.6, resulting in a reversible reaction that is slightly displaced towards the production of NADPH. For the C266A and C266A/L268A variants this ratio considerably increases favouring the oxidation of the protein. In the double mutant, the determined values of k_{HT-1} were approximately 30-fold higher than the values of k_{HT}. These observations are in agreement with the differences observed for the stabilisation of oxidised and reduced species in equilibrium after the HT event, and with the obtained $E_{ox/hq}$ values (Table 2). Thus, the FNR variants showing more negative midpoint potentials and, therefore, more distant to the $E_{NADP+/NADPH}$ value show a displacement in the equilibrium towards the reduced form of the coenzyme.

The crystal structure here obtained for C266M indicates that the mutation generates a volume increase in this particular side-chain, but does not change the overall structure of the enzyme, including the conserved FAD conformation. However, the C-terminal β-sheet (from W303 to the Y308 carboxyl terminus) is slightly displaced, probably to accommodate the introduced methionine that causes i) the displacement of E306 away from M266 and S90 and ii) slightly larger flexibility in the environment of the mutation (Fig. 6). Although we do not have at our disposal the structures of the rest of the mutants at position 266, we can assume that the interaction network between E306 and the surrounding residues at the active site must be also altered. It has been previously observed that in the *Anabaena* WT enzyme the loop corresponding to this region moves upon binding of $NADP^+$ to allow a perfect complementarity between the nucleotide substrate and the protein [32]. The C266M structure suggests a contribution of the replaced aminoacid in the E306 conformation, a residue critical for semiquinone stabilisation, proper binding of the nicotinamide ring into the active centre, CTC stabilisation and efficient flavin reduction by NADPH [6,33,34]. Moreover, several evidences point to this glutamate as responsible of transferring protons from the external medium to the buried N5i atom via the hydroxyl group of S90 [6,12,35–38]. The conformation of this glutamic acid should be properly adjusted to perform this dual role: to act as a proton shuttle/donor and to stabilise the semiquinone during catalysis. In our mutants the bulky side-chain of the Met introduced at 266 forced the glutamic acid side-chain to move further away from S90 and closer to the flavin, distorting the interaction with the serine and the flavin and, therefore, affecting both roles. In the same way, smaller side-chains as in the C266A mutant might increase the freedom of the glutamic side-chain, allowing it to acquire nonoptimal conformations for proton transfer. Consequently, mutation C266A will impede optimal interaction of the E306 carboxylate with S90, affecting the HT capability by inhibiting the flavin protonation/deprotonation step. An

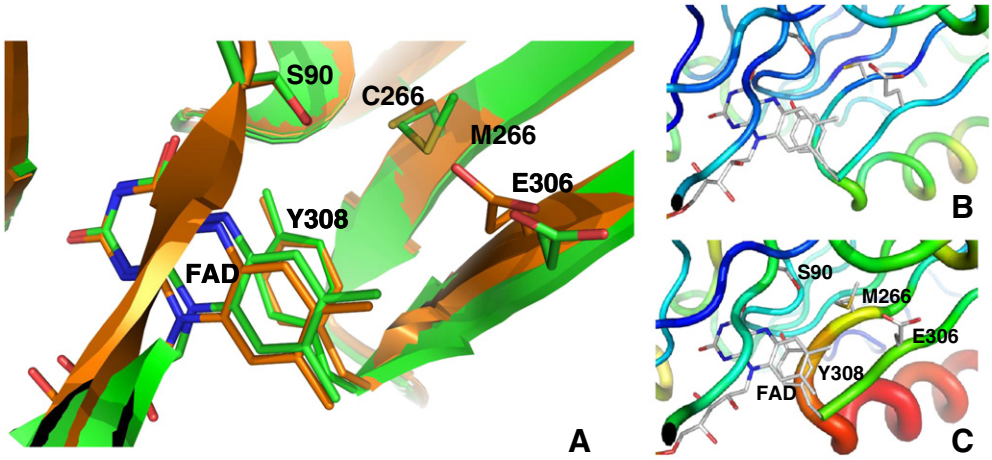

Fig. 6. Comparison at the active site environment of the crystal structures of WT and C266M pea FNRs. (A) Cartoon detail of the superposition of C266M FNR (in green) and the WT FNR (in orange) structures. Cartoon representation of the α-carbon B-factors for the (B) WT and (C) C266M pea FNRs. Positions with larger fluctuations are indicated in wide cartoon and red colour, while those with the lower fluctuation are shown as the thin cartoon and blue colour. Intermediate fluctuations range from wide to thin cartoons and red to blue colours. The FAD and the side-chains of S90, C/M266, E306, and Y308 are in sticks and CPK coloured.

unforeseen result that may help to support our hypothesis is the detection of stabilised semiquinone upon HT with the coenzyme in the mutant C266A. In this mutant the glutamate might be more prone to stabilise the semiquinone than to exchange protons with the serine–flavin pair, inducing the observed effect, as it has also been observed by mutations introduced in other flavoenzymes [29,39]. Thus, in conclusion HT decreases because the mutations impede the formation of the catalytically competent encounter between the reacting rings.

The L268V mutant showed the same behaviour as the WT enzyme for the coenzyme affinity and a moderate reduction of the catalytic efficiency in steady-state measurements [14] and, similar results are observed for the intermediate species and transient-rate constants when studying the transient reaction of FNR_{ox} with NADPH. Replacement of the equivalent Leu (L263) by an Ala in *Anabaena* FNR only produced a minor deleterious effect in the catalytic efficiency, but when a Pro was substituted for the Leu more drastic effects in both nicotinamide allocation and HT parameters were observed [40]. Crystal structures of L268V pea and L263P *Anabaena* FNRs only show differences restricted to the mutated side-chain regarding their corresponding WT forms. Changes in volume at this Leu appear to have a considerably smaller influence on HT rates than in the above mentioned Cys, and no clear correlation can be extracted (Fig. 5B). Introduction of the Pro produces a stronger deleterious effect, but it might be related with a tighter conformation of the 260's sequence. Upon binding of $NADP^+$ to FNR less extended conformations have been reported, in which the hydrophobic side-chain of this Leu contributes through van der Waals contacts to place both nucleotide moieties of the $NADP^+$; on one side it clamps the ribose and the nicotinamide portion and on the other the adenine ring of the adenosine nucleotide [9,10,12,32]. According to the available data obtained through the different mutations at this position, neither the volume of the residue nor the interactions established by the side-chain are critical to attain the catalytically competent complex. However, the flexibility of its backbone appears more important for an efficient catalysis. This is in agreement with a Pro being the preferred residue in the NAD^+-dependent members of the FNR family that use a preformed binding site for the nucleotide, while $NADP^+$ dependent members, as FNR itself, require a series of concerted conformational changes that include those at the 260's sequence [13,40].

The data here presented indicate that the interaction with the coenzyme and in consequence the HT process is highly disrupted by volume changes at position 266 of pea FNR. However, backbone flexibility at position 268 appears to be the most critical factor to attain the catalytically competent complex. Our results allow a better understanding of how the architecture of the catalytically competent complex is precisely formed between FNR and the $NADP^+$/H to make this enzyme so efficient in catalysis.

Acknowledgements

This work was supported by the Ministerio de Ciencia e Innovación, Spain (grant BIO2010-14983 to M.M.), ANCYPT, Ministerio de Ciencia, Tecnología e Innovación Productiva (ANCYPT PICT-2007 01–00645) and Consejo Nacional de Investigaciones Científicas y Técnicas (PIP 252), Argentina.

References

[1] A. Aliverti, V. Pandini, A. Pennati, M. de Rosa, G. Zanetti, Structural and functional diversity of ferredoxin-$NADP^+$ reductases, Arch. Biochem. Biophys. 474 (2008) 283–291.
[2] D.H. Paladini, M.A. Musumeci, N. Carrillo, E.A. Ceccarelli, Induced fit and equilibrium dynamics for high catalytic efficiency in ferredoxin-NADP(H) reductases, Biochemistry 48 (2009) 5760–5768.
[3] A. Bortolotti, I. Pérez-Dorado, G. Goñi, M. Medina, J.A. Hermoso, N. Carrillo, N. Cortez, Coenzyme binding and hydride transfer in *Rhodobacter capsulatus* ferredoxin/flavodoxin NADP(H) oxidoreductase, Biochim. Biophys. Acta 1794 (2009) 199–210.
[4] C.J. Batie, H. Kamin, Electron transfer by ferredoxin:$NADP^+$ reductase. Rapid-reaction evidence for participation of a ternary complex, J. Biol. Chem. 259 (1984) 11976–11985.
[5] I. Lans, J.R. Peregrina, M. Medina, M. Garcia-Viloca, A. Gonzalez-Lafont, J.M. Lluch, Mechanism of the hydride transfer between *Anabaena* Tyr303Ser FNR(rd)/FNR(ox) and NADP(+)/H. A combined pre-steady-state kinetic/ensemble-averaged transition-state theory with multidimensional tunneling study, J. Phys. Chem. B 114 (2010) 3368–3379.
[6] J.R. Peregrina, A. Sánchez-Azqueta, B. Herguedas, M. Martínez-Júlvez, M. Medina, Role of specific residues in coenzyme binding, charge-transfer complex formation, and catalysis in *Anabaena* ferredoxin $NADP^+$-reductase, Biochim. Biophys. Acta 1797 (2010) 1638–1646.
[7] J. Tejero, J.R. Peregrina, M. Martínez-Júlvez, A. Gutiérrez, C. Gómez-Moreno, N.S. Scrutton, M. Medina, Catalytic mechanism of hydride transfer between $NADP^+$/H and ferredoxin-$NADP^+$ reductase from *Anabaena* PCC 7119, Arch. Biochem. Biophys. 459 (2007) 79–90.
[8] M. Ortiz-Maldonado, B. Entsch, D.P. Ballou, Conformational changes combined with charge-transfer interactions are essential for reduction in catalysis by p-hydroxybenzoate hydroxylase, Biochemistry 42 (2003) 11234–11242.
[9] J. Tejero, I. Pérez-Dorado, C. Maya, M. Martínez-Júlvez, J. Sanz-Aparicio, C. Gómez-Moreno, J.A. Hermoso, M. Medina, C-terminal tyrosine of ferredoxin-$NADP^+$ reductase in hydride transfer processes with $NAD(P)^+$/H, Biochemistry 44 (2005) 13477–13490.
[10] Z. Deng, A. Aliverti, G. Zanetti, A.K. Arakaki, J. Ottado, E.G. Orellano, N.B. Calcaterra, E.A. Ceccarelli, N. Carrillo, P.A. Karplus, A productive $NADP^+$ binding mode of ferredoxin-$NADP^+$ reductase revealed by protein engineering and crystallographic studies, Nat. Struct. Biol. 6 (1999) 847–853.
[11] L. Piubelli, A. Aliverti, A.K. Arakaki, N. Carrillo, E.A. Ceccarelli, P.A. Karplus, G. Zanetti, Competition between C-terminal tyrosine and nicotinamide modulates pyridine nucleotide affinity and specificity in plant ferredoxin-$NADP^+$ reductase, J. Biol. Chem. 275 (2000) 10472–10476.
[12] J.R. Peregrina, I. Lans, M. Medina, The transient catalytically competent coenzyme allocation into the active site of *Anabaena* ferredoxin NADP(+)-reductase, Eur. Biophys. J. 41 (2012) 117–128.
[13] J.R. Peregrina, B. Herguedas, J.A. Hermoso, M. Martínez-Júlvez, M. Medina, Protein motifs involved in coenzyme interaction and enzymatic efficiency in *Anabaena* ferredoxin-$NADP^+$ reductase, Biochemistry 48 (2009) 3109–3119.
[14] M.A. Musumeci, A.K. Arakaki, D.V. Rial, D.L. Catalano-Dupuy, E.A. Ceccarelli, Modulation of the enzymatic efficiency of ferredoxin-NADP(H) reductase by the amino acid volume around the catalytic site, FEBS J. 275 (2008) 1350–1366.
[15] M.B. Murataliev, R. Feyereisen, F.A. Walker, Electron transfer by diflavin reductases, Biochim. Biophys. Acta 1698 (2004) 1–26.
[16] E.A. Ceccarelli, A.K. Arakaki, N. Cortez, N. Carrillo, Functional plasticity and catalytic efficiency in plant and bacterial ferredoxin-NADP(H) reductases, Biochim. Biophys. Acta 1698 (2004) 155–165.
[17] I. Nogués, L.A. Campos, J. Sancho, C. Gómez-Moreno, S.G. Mayhew, M. Medina, Role of neighboring FMN side chains in the modulation of flavin reduction potentials and in the energetics of the FMN:apoprotein interaction in *Anabaena* flavodoxin, Biochemistry 43 (2004) 15111–15121.
[18] S. Frago, G. Goñi, B. Herguedas, J.R. Peregrina, A. Serrano, I. Pérez-Dorado, R. Molina, C. Gómez-Moreno, J.A. Hermoso, M. Martínez-Júlvez, S.G. Mayhew, M. Medina, Tuning of the FMN binding and oxido-reduction properties by neighboring side chains in *Anabaena* flavodoxin, Arch. Biochem. Biophys. 467 (2007) 206–217.
[19] S. Frago, I. Lans, J.A. Navarro, M. Hervás, D.E. Edmondson, M.A. De la Rosa, C. Gómez-Moreno, S.G. Mayhew, M. Medina, Dual role of FMN in flavodoxin function: electron transfer cofactor and modulation of the protein–protein interaction surface, Biochim. Biophys. Acta 1797 (2010) 262–271.
[20] W. Kabsch, XDS, Acta Crystallogr. D: Biol. Crystallogr. 66 (2010) 125–132.
[21] E. Potterton, P. Briggs, M. Turkenburg, E. Dodson, A graphical user interface to the CCP4 program suite, Acta Crystallogr. D: Biol. Crystallogr. 59 (2003) 1131–1137.
[22] N. Collaborative Computational Project, The CCP4 suite: programs for protein crystallography, Acta Crystallogr. D50 (1994) 760–763.
[23] A. Vagin, A. Teplyakov, MOLREP: an automated program for molecular replacement, J. Appl. Crystallogr. 30 (1997) 1022–1025.
[24] G.N. Murshudov, A.A. Vagin, E.J. Dodson, Refinement of macromolecular structures by the maximum-likelihood method, Acta Crystallogr. D: Biol. Crystallogr. 53 (1997) 240–255.
[25] B. Howlin, S.A. Butler, D.S. Moss, G.W. Harris, H.P.C. Driessen, TLSANL: TLS parameter analysis program for segmented anisotropic refinement of macromolecular structures, J. Appl. Crystallogr. 26 (1993) 622–624.
[26] P. Emsley, K. Cowtan, Coot: model-building tools for molecular graphics, Acta Crystallogr. D: Biol. Crystallogr. 60 (2004) 2126–2132.
[27] R.A. Laskowski, M.W. MacArthur, D.S. Moss, J.M. Thornton, PROCHECK: a program to check the stereochemical quality of protein structures, J. Appl. Crystallogr. 26 (1993) 283–291.
[28] S.C. Lovell, I.W. Davis, W.B. Arendall III, P.I. de Bakker, J.M. Word, M.G. Prisant, J.S. Richardson, D.C. Richardson, Structure validation by Calpha geometry: phi, psi and Cbeta deviation, Proteins 50 (2003) 437–450.
[29] K.J. McLean, N.S. Scrutton, A.W. Munro, Kinetic, spectroscopic and thermodynamic characterization of the *Mycobacterium tuberculosis* adrenodoxin reductase homologue FprA, Biochem. J. 372 (2003) 317–327.
[30] J.D. Lambeth, H. Kamin, Adrenodoxin reductase. Properties of the complexes of reduced enzyme with $NADP^+$ and NADPH, J. Biol. Chem. 251 (1976) 4299–4306.

[31] S. Daff, An appraisal of multiple NADPH binding-site models proposed for cytochrome P450 reductase, NO synthase, and related diflavin reductase systems, Biochemistry 43 (2004) 3929–3932.
[32] J.A. Hermoso, T. Mayoral, M. Faro, C. Gomez-Moreno, J. Sanz-Aparicio, M. Medina, Mechanism of coenzyme recognition and binding revealed by crystal structure analysis of ferredoxin-NADP$^+$ reductase complexed with NADP$^+$, J. Mol. Biol. 319 (2002) 1133–1142.
[33] A. Aliverti, Z. Deng, D. Ravasi, L. Piubelli, P.A. Karplus, G. Zanetti, Probing the function of the invariant glutamyl residue 312 in spinach ferredoxin-NADP$^+$ reductase, J. Biol. Chem. 273 (1998) 34008–34015.
[34] M. Medina, M. Martínez-Júlvez, J.K. Hurley, G. Tollin, C. Gómez-Moreno, Involvement of glutamic acid 301 in the catalytic mechanism of ferredoxin-NADP$^+$ reductase from *Anabaena* PCC 7119, Biochemistry 37 (1998) 2715–2728.
[35] G. Kurisu, M. Kusunoki, E. Katoh, T. Yamazaki, K. Teshima, Y. Onda, Y. Kimata-Ariga, T. Hase, Structure of the electron transfer complex between ferredoxin and ferredoxin-NADP$^+$ reductase, Nat. Struct. Biol. 8 (2001) 117–121.
[36] M. Medina, R. Abagyan, C. Gómez-Moreno, J. Fernández-Recio, Docking analysis of transient complexes: interaction of ferredoxin-NADP$^+$ reductase with ferredoxin and flavodoxin, Proteins 72 (2008) 848–862.
[37] R. Morales, M.H. Charon, G. Kachalova, L. Serre, M. Medina, C. Gómez-Moreno, M. Frey, A redox-dependent interaction between two electron-transfer partners involved in photosynthesis, EMBO Rep. 1 (2000) 271–276.
[38] V.I. Dumit, T. Essigke, N. Cortez, G.M. Ullmann, Mechanistic insights into ferredoxin-NADP(H) reductase catalysis involving the conserved glutamate in the active site, J. Mol. Biol. 397 (2010) 814–825.
[39] M. Sabri, A.J. Dunford, K.J. McLean, R. Neeli, N.S. Scrutton, D. Leys, A.W. Munro, Characterization of coenzyme binding and selectivity determinants in *Mycobacterium tuberculosis* flavoprotein reductase A: analysis of Arg(199) and Arg(200) mutants at the NADP(H) 2′-phosphate binding site, Biochem. J. 417 (2009) 103–112.
[40] J. Tejero, M. Martínez-Júlvez, T. Mayoral, A. Luquita, J. Sanz-Aparicio, J.A. Hermoso, J.K. Hurley, G. Tollin, C. Gómez-Moreno, M. Medina, Involvement of the pyrophosphate and the 2′-phosphate binding regions of ferredoxin-NADP$^+$ reductase in coenzyme specificity, J. Biol. Chem. 278 (2003) 49203–49214.
[41] I. Nogués, J. Tejero, J.K. Hurley, D. Paladini, S. Frago, G. Tollin, S.G. Mayhew, C. Gómez-Moreno, E.A. Ceccarelli, N. Carrillo, M. Medina, Role of the C-terminal tyrosine of ferredoxin-nicotinamide adenine dinucleotide phosphate reductase in the electron transfer processes with its protein partners ferredoxin and flavodoxin, Biochemistry 43 (2004) 6127–6137.
[42] M.E. Corrado, A. Aliverti, G. Zanetti, S.G. Mayhew, Analysis of the oxidation-reduction potentials of recombinant ferredoxin-NADP$^+$ reductase from spinach chloroplasts, Eur. J. Biochem. 239 (1996) 662–667.
[43] M. Faro, C. Gómez-Moreno, M. Stankovich, M. Medina, Role of critical charged residues in reduction potential modulation of ferredoxin-NADP$^+$ reductase, Eur. J. Biochem. 269 (2002) 2656–2661.